A Microbeam Slit System for High Beam Currents

Thomas Vallentin 2014

Master thesis

A Microbeam Slit System for High Beam Currents

Institut für Angewandte Physik und Messtechnik LRT2
Fakultät für Luft- und Raumfahrttechnik
Universität der Bundeswehr München

Erstprüfer: Univ.-Prof. Dr. rer. nat. Günther Dollinger
Zweitprüfer: Dr. rer. nat. Patrick Reichart
Betreuer: M.Sc. Marcus Moser

Vorgelegt von:

Thomas Vallentin
Werner-Heisenberg-Weg 117
85579 Neubiberg
Telefon: +49 1578 2548451
E-Mail: thomas.vallentin@unibw.de
Matrikelnummer: 1100449

Selbstständigkeitserklärung

Hiermit erkläre ich, dass ich die vorliegende Masterarbeit selbstständig und nur unter Zuhilfenahme der angegebenen Quellen erstellt habe. Außerdem habe ich die Zitate ordnungsgemäß gekennzeichnet und keine anderen als die im Literatur-/Schriftenverzeichnis angegebenen Quellen und Hilfsmittel benutzt.

Datum und Ort

Thomas Vallentin

Einverständniserklärung

Hiermit erkläre ich mich damit einverstanden, dass die vorliegende Masterarbeit auf den Internetpräsenzen der Universität der Bundeswehr München sowie der Arbeitsgruppe SNAKE unverändert veröffentlicht werden darf.

Datum und Ort

Thomas Vallentin

Contents

Abstract

A new microbeam slit system for high beam currents of 10 µA was built up to improve the brightness transport of a proton beam with a kinetic energy of up to 25 MeV into the microprobe SNAKE.

The new slit system features a position accuracy of less than 1 µm under normal operating conditions and less than 2 µm if the beam is switched on and off [1]. The thermal management with a powerful watercooling and potential-free thermocouple feedback controlled heating cables is optimized for constant slit aperture. The transparent zone is reduced to 0.7 µm due to the use of mechanically lapped tungsten as slit tip material to reduce small angle scattering effects and to reduce the number of ions passing the slits with low energy loss. The slits feature electrical isolation of the slit tip to make slit current monitoring possible, e.g. for tandem feedback control.

With the high possible thermal power input of 250 W we could measure for the first time the high-energy beam brightness B_{exp} of injected beams with high emittances of $\epsilon_{in} = 2\pi$ mm mrad. The brightness B_{exp} transported into the microprobe was improved to $B_{exp} = 2\,\mu A/(mm^2\,mrad^2\,MeV)$ and therefore brightness loss through the tandem accelerator was around 25 %. The higher transported brightness B_{exp} gives the opportunity to achieve the high resolution of the single ion, cell irradiation setup [8, 7] ($\approx$ 320 nm) also at higher current of $I_{exp} = 100$ pA for materials analysis [5].

1 Introduction

Microprobe resolution can be improved by decreasing the aperture and thus the accepted angles $\langle \theta_x, \theta_y \rangle$ of the microlens system for smaller lens aberrations [9] and the object sizes $\langle \Delta x, \Delta y \rangle$ for a smaller object diameter. However, sufficient beam current $I_{exp} > 100\,pA$ [5] is needed at the microprobe for acceptable measuring time, e.g. for 3D hydrogen microscopy by pp-scattering [4].
As a consequence of the smaller acceptance $\epsilon_{SNAKE} = \Delta x \cdot \Delta y \cdot \theta_x \cdot \theta_y$ of the microprobe, a higher beam brightness $B = I_{exp}/(\epsilon E)$ is needed to keep the same beam current I_{exp}. Therefore, we installed a new MultiCUSP ion source at the Munich MP Tandem with a brightness of $B = 27\,\mu A/(mm^2\,mrad^2\,MeV)$ (measured at test bench), which is capable of producing H^- beams with more than 200 times more ions in the same phase space compared to the one it replaced [3].
As reported in [3] there is a leak between the brightness of the ion source, the injected and the transported brightness. One main reason is that the injected and transported beam current has to be limited because the original microslit system cannot handle thermal loads of more than $\dot{Q} = 10\,W$ [1]. To avoid this problem we reduced the phase space to fulfill the max. 10 W power restriction on our original microslit system. However, when reducing the acceptance of the tandem that much, the transported brightness is reduced by geometrical constraints and by small angle scattering effects from the terminal stripping foil [3]. Thus, beam brightness at SNAKE could only be improved to $B = 0.8\,\mu A/(mm^2\,mrad^2\,MeV)$ [3]. In order to allow for higher brightness at SNAKE, a new slit system has been constructed that fulfills all necessary requirements, as described in the following section. A sketch of the newly constructed slit system is shown in fig. 1.

2 System description

2.1 Temperature management

Safety requirements allow a maximum of 10 µA proton beam current to be injected into the Munich MP Tandem. For 25 MeV ions this results in a thermal power load of up to 250 W on the microslit system, which has to be dissipated. A watercooling with 250 W heat dissipation [1] is used to control this thermal load. The entire water channel geometry and mass flow are designed for laminar flow condition (Reynolds number $Re < 2000$) in order to prevent micro-vibration induced stall [1] and the water flow is realized by static pressure only.

2.2 Mechanical slit control

For the microprobe operation as object slits, slit aperture and slit position have to be controlled with a precision better than 2 µm. A stepping motor translational stage is used to obtain this mechanical precision. Furthermore, a vibration isolation from the beam tube (that is subject to a high vibration load from mechanical pumps and the tandem) maintains this level of precision via elastic bellows in absolute position. Hence, the microslits are mechanically decoupled from the vibrating beam tube.
As a solution to stabilize the temperature profile and therefore thermal expansions through beam load jitter, a powerful preheating is used as before with the existing slits [6]. However, heating of the top is not possible due to the electrical isolation for slit current monitoring. Therefore we use potential-free heating cables, which provide the desired power of 250 W per slit and give enough electrical isolation between heating current supply and heated material, so that beam current measurement is not affected [1]. For optimum heat conduction we use a 100 µm thick gold foil between removable copper parts. All heat transporting non removable parts have been hard-soldered with high heat conducting solder and soldering areas only in parallel to the heat fluxes during operation. The temperature of the copper heater (fig. 1 'C') can be held constant via thermocouple feedback control to ensure low thermal expansions during operation.

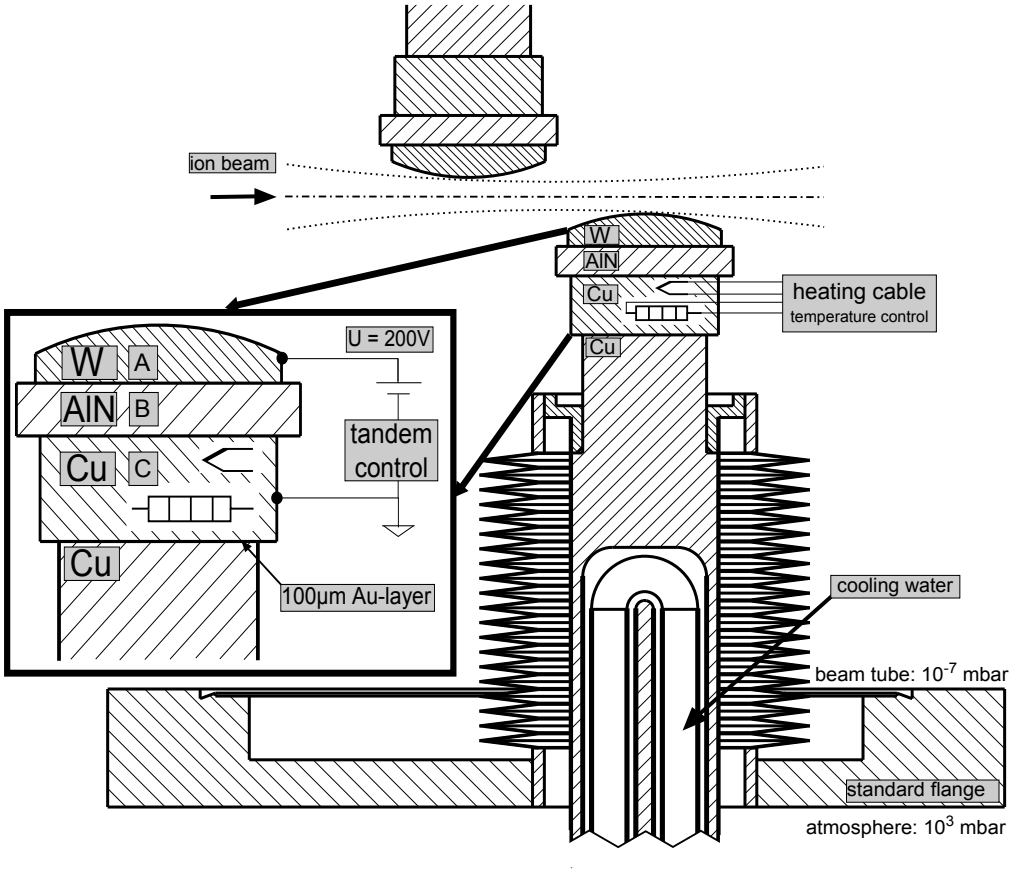

Figure 1: Sectional view of the new microslit system. The top of the slit half consists of a tungsten slit bracket (A), aluminum nitride isolation ceramic (B) and temperature controlled copper heater (C). The top is thermally coupled via a 100 µm gold layer to a copper bar. This bar is composed of to halves with the cooling water tubes curved in. This bar is also uncoupled to the beam tube via bellows. The copper heater (C) uses heating cables and thermocouples for temperature control. The beam current is measured at the tungsten bracket. This bracket is lifted to U = 200 V in order to avoid secondary electron escape.

2.3 Slit surface properties

Further requirements for microprobe operation are a minimum of slit scattering by reduction of the transparent zone as well as a minimum of surface roughness [6]. A minimal transparent zone can be achieved by using heavy elements as slit tip material, because the stopping is much higher. Therefore, we use mechanically lapped tungsten at a cylindrical geometry with a top radius of r = 100 mm as slit tip material. This results in a transparent zone thickness of 0.7 µm at 25 MeV protons for the new microslit system. The old microslits using a silicon wafer bended to r = 50 mm radius [6] have 30 µm transparent zone thickness at 25 MeV protons. Hence, the transparent zone is reduced with the new microslits to $< 3\,\%$.
Other reasons to use tungsten as slit tip material [1] are the high thermal conductivity of $k_W = 160\,W/(m\,K)$ and low thermal expansion of $\alpha_{th,W} = 4.3 \times 10^{-6}/K$ for $T < 400\,°C$. Furthermore it has a low sputter erosion rate because of its high melting and boiling point. For radiation safety reasons it also offers a moderate activation of long lifetime radioisotopes due to nuclear reactions from the beam interactions.
For a precise defined object and therefore for a sharper beam profile, the slit surface has to be ideally atomically flat, as it was using silicon wafers. Hence the radial tungsten slit surface has been mechanically lapped to an average roughness of Ra = 0.016 µm, which is optically specular, remaining in its circular geometry.

2.4 Slit current monitoring

The existing slits for tandem regulation are located just 30 cm in front of the SNAKE microslits. However, with the new high brightness source, the slit current often becomes unstable because of beam fluctuations by sweeping the (non-uniformly distributed) beam over the few µm opened microslits. Loss of optimum brightness is the consequence. Hence, the microslits themselves have to be used as tandem control slits. Precise current measurement of µA or nA current demands an optimal electrically isolated slit tip and leakage current from heating smaller than 1 nA.
To combine the high heat input with the ability to measure low nA currents, we use a ceramic isolation by 6 mm thick aluminum nitride (fig. 1 'A'), which combines a specific electrical resistance of $\rho_v = 5 \times 10^5\,\Omega\,m$ at $T = 400\,°C$ [12] and a sufficient thermal conductivity of up to $k_{AlN} = 180\,W/(m\,K)$. This results in an electrical isolation resistance of $R \approx 10^7\,\Omega$. A clip construction provides optimum heat contact. Preheating of the top parts of the slits (fig. 1 'A' and 'B') is impossible due to the required electrical isolation for current measurement. Hence we heat the copper bar (fig. 1 'C') and use materials with low thermal expansion at the top parts, which is applicable for aluminum nitride and tungsten.

3 Performance of new slits

3.1 Temperature stability

The thermal stability of the new slits was tested with 20 MeV protons from the new high brightness MultiCUSP source. Limited by the accelerator, a current of max. 8.7 µA has been transported to the slits, which is about 10 times more than the maximum average current capable by the old slits. At this current, the temperature was kept stable at $\vartheta_\mathrm{p} = (100 \pm 0.1)°\mathrm{C}$ by preheating with heating cables and thermocouple feedback control. The water cooling with $\vartheta_\mathrm{w} = (15 \pm 1)°\mathrm{C}$ feed temperature was active at this time. The temperature uncertainties $\Delta\vartheta_\mathrm{p}, \Delta\vartheta_\mathrm{w}$ result in an uncertainty of slit aperture from thermal expansion of less than 1 µm [1]. However, if the beam load is switched on and off, thermal expansion is in the range of 2 µm for less than $t = 10\,\mathrm{s}$ until the beam load is equally distributed on the slits [1]. Fluctuations of the object size and position due to vibrations of the water cooling pipes have not been observed so far. The influence of slit position uncertainty in the range of 1 µm to 2 µm can be tolerated for slit apertures in the range of 10 µm to 20 µm. As a result, the new concept has been proven to fulfill the requirements.

3.2 Tandem control

With the new slitsystem we are able to give high current load on the slits and use the high feedback current directly from the microslits. So far, the feedback system has proven to work up to a load of about 5 µA. Due to the control system adapted to lower currents, the tandem voltage control became unstable. The slit current monitors will be rebuilt in future in order to use the high feedback current of the new slits to stabilize the tandem terminal voltage at higher beam currents.

3.3 Brightness analysis with new microslits

An increase of transported brightness is accompanied directly with an increase of possible microprobe resolution [14]. The new microslit system enables for the first time to measure brightness with high injection current. Therefore much attention was turned to the brightness determination behind the new microslit system, which is the brightness transported into SNAKE. We have to assume isotropic filled apertures, so brightness can be determined to [13]

$$B = \frac{I_{exp}}{A_{obj}\frac{A_{div}}{(l_{div})^2}E_{ion}} \tag{1}$$

with the beam current I_{exp} measured on target cup of SNAKE 30 m behind the microslits [3], the rectangular microslit object size $A_{obj} = \Delta x_{obj} \cdot \Delta y_{obj}$ as the product of the slit apertures of the new microslit system, the divergence angles $\langle \theta_x, \theta_y \rangle$ with the divergence size $\frac{A_{div}}{l^2} = \frac{\Delta x_{div}}{l} \cdot \frac{\Delta y_{div}}{l}$ as the product of the slit apertures of the divergence slits, which are located $l_{div} = 5.5\,\mathrm{m}$ behind the object slits, and the kinetic energy of the ion beam $E_{ion} = 20\,\mathrm{MeV}$.
For optimum beam preparation on the low-energy stage of the tandem facility, the beam current was optimized to $I_{in} = 18.5\,\mu\mathrm{A}$ under an injection half-angle of $\theta_{in} = 2.08\,\mathrm{mrad}$ and radius of $r_{in} = 0.96\,\mathrm{mm}$ with circular apertures. This results in an injection brightness of $B = 2.8\,\mu\mathrm{A}/(\mathrm{mm}^2\,\mathrm{mrad}^2\,\mathrm{MeV})$ at 180 keV. In fact, this is a factor of 10 lower than expected, but it is due to non-optimal transport characteristics and injection conditions of the source with an original brightness of up to $B = 27\,\mu\mathrm{A}/(\mathrm{mm}^2\,\mathrm{mrad}^2\,\mathrm{MeV})$ at 30 keV in test conditions [3].
The results of the measured injected brightness on the low-energy side of the tandem are printed in fig. 2. This figure shows the injected brightness B_{in} against the injection diameter r_{in} in a) for different injection angles θ_{in}. In b) the injected brightness B_{in} is shown against the injection angle θ_{in} for different injection diameters r_{in}. Brightness has been calculated via the measured current I_{exp} on a Faraday cup via eqn. (1), with the object and divergence areas as the areas of the opening of the circular low-energy apertures before the tandem accelerator at an injection energy of 180 keV. On gross scale the brightness remains pretty constant for all beam settings. The slight decrease in beam brightness at larger slit apertures may be due to slight inhomogeneity in the current density. The slight decrease of beam brightness at small object sizes r_{in} might be due to uncertainties of the aperture size.
The results for the high-energy brightness determination are printed in fig. 3. Shown is the experimental brightness B_{exp} against the object area of the new microslit system

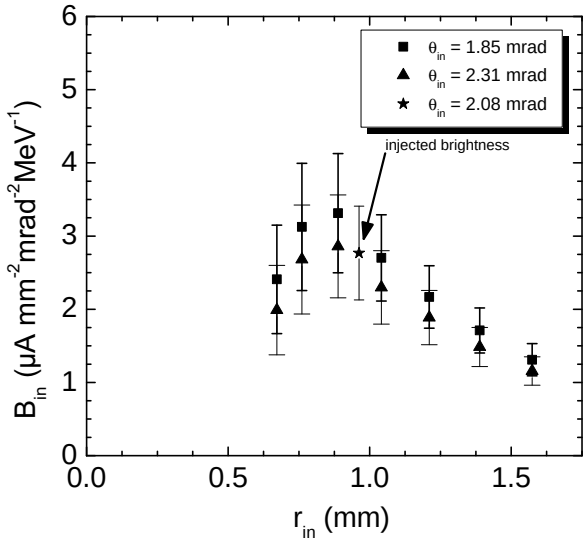

(a)

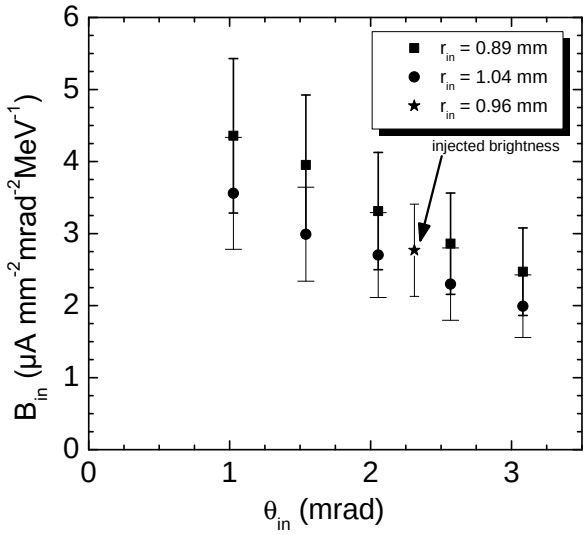

(b)

Figure 2: Measured injected brightness distribution on the low-energy side of the Munich MP tandem injection. The injected brightness B_{in} is shown depending of the injection diameter r_{in} in a) for different injection angles θ_{in}. In b) the injected brightness B_{in} is shown against the injection angle θ_{in} for different injection diameters r_{in}. Brightness has been calculated via the measured current I_{exp} on a Faraday cup via eqn. (1), with the object and divergence areas as the areas of the aperture of the circular low-energy apertures before the tandem accelerator at an injection energy of 180 keV. The optimum beam condition for high-energy brightness transport is marked with an arrow.

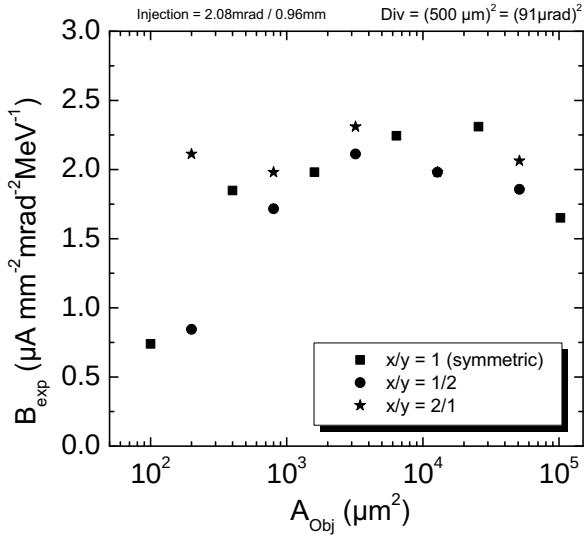

(a)

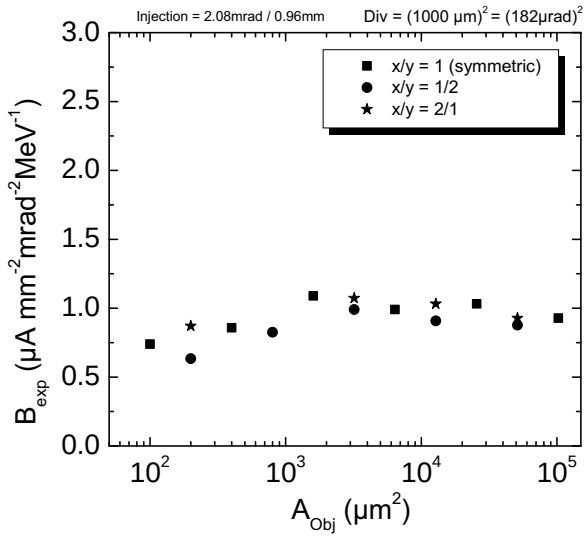

(b)

Figure 3: Measured experimental brightness distribution on the high-energy stage after the energy selecting magnet. Experimental brightness B_{exp} is shown depending of the object area of the new microslit system $A_{obj} = \Delta x_{obj} \cdot \Delta y_{obj}$ at a divergence $\theta = \theta_x \cdot \theta_y$ of $(91\,\mu rad)^2$ full-angle in a), and at divergence of $(182\,\mu rad)^2$ full-angle in b). In both cases, the ion beam was injected with an emittance of $\epsilon_{in} = 2\pi\,mm\,mrad$, marked with an arrow in fig. 2.

A_{obj} at a divergence of $(91\,\mu rad)^2$ in a), and at divergence of $(182\,\mu rad)^2$ in b). We injected a pulsed proton beam with a brightness of $B = 2.8\,\mu A/(mm^2\,mrad^2\,MeV)$ at 180 keV with $\epsilon_{in} = \theta_{in} \cdot r_{in} \cdot \pi = 2\pi\,mm\,mrad$ into the tandem (arrow in fig. 2).
With the injected emittance ϵ_{in}, the brightness has been improved up to $B \approx 2\,\mu A/(mm^2\,mrad^2\,MeV)$ at SNAKE, as shown in fig. 3. At divergence of $(91\,\mu rad)^2$, brightness is around $B \approx 2\,\mu A/(mm^2\,mrad^2\,MeV)$ for most object sizes and thus 25 % lower than the injected brightness. Since stripper efficiency to the 1^+ charge state is limited to 80 % when using a $4\,\mu g/m^2$ carbon stripper foil at the 10 MV terminal of the tandem [10], the measured high energy beam brightness shows a complete transport of beam brightness from the low energy side to the high energy side of Munich MP tandem [**?**].
At the new microslits, brightness is little higher in x-direction for asymmetric x/y-proportion, which is mostly dependent to beam transport through the tandem. Only at small object sizes as $A_{obj} \approx 10\,\mu m \times 10\,\mu m$ we see significantly reduced brightness. This is also influenced by the axial shifting of the two x-slit-halves, which causes an inhomogeneous divergence distribution. Therefore the second x-slit tip lowers the divergence of the beam in one direction.
For greater divergence of $(182\,\mu rad)^2$ we measure lower brightness of only $B \approx 1\,\mu A/(mm^2\,mrad^2\,MeV)$ at SNAKE, as shown in fig. 3 b). We assume this is mostly due to non-isotropic illumination of the microslits in the angle phase space (see fig. 2 b)), but this could be compensated with larger injection angles θ_{in}.

3.4 Microprobe resolution

With a transported brightness of $B \approx 2\,\mu A/(mm^2\,mrad^2\,MeV)$ a resolution increase is possible. We calculate the possible object size with eqn. (1) to

$$A_{obj} = \frac{I_{exp}}{B_{exp}\frac{A_{div}}{(l_{div})^2}E_{ion}} \tag{2}$$

with the transported brightness $B \approx 2\,\mu A/(mm^2\,mrad^2\,MeV)$, the needed beam current $I_{exp} = 100\,pA$ measured on target cup of SNAKE, the divergence size $A_{div} = \Delta x_{div} \cdot \Delta y_{div} = 470\,\mu m \cdot 300\,\mu m$ as the slit wides of the divergence slits, which are located $l_{div} = 5.5\,m$ behind the object slits, and the kinetic energy of the ion beam $E_{ion} = 20\,MeV$. The divergence slit sizes are adapted to result in less than 25 % lens aperture of the total [7]. Because of asymmetric demagnification and beam entrance angles, the divergence size is also asymmetric. The possible object size can be calculated to $A_{obj} = \Delta x_{obj} \cdot \Delta y_{obj} = 530\,\mu m^2$.

For a single stage projection of the object we have demagnification in x-direction of 35 and in y-direction of 206 [7]. For an optimum symmetric beam spot on the target we get object slit wides of $\Delta x_{obj} = 10\,\mu m$ in x-direction and $\Delta y_{obj} = 56\,\mu m$ in y-direction. This results in a theoretical lateral resolution in x- and y-direction of $\Delta x_{SNAKE} \times \Delta y_{SNAKE} \approx 280\,nm \times 280\,nm$.

Even smaller beam spot size is possible with lens aperture below 12.5 % of the total, as shown in [7]. If we calculate the theoretical lateral resolution with the same parameters as above but with the smaller lens illumination, it results in $\Delta x_{SNAKE} \times \Delta y_{SNAKE} \approx 550\,nm \times 550\,nm$. However the best measured results in [7] are $\Delta x_{SNAKE} \times \Delta y_{SNAKE} = 1600\,nm \times 320\,nm$. This resolution can only be increased by smaller lens projection aberrations and reduced parasitic effects, e.g. fluctuating magnetic fields (e.g. 50Hz). It is not limited by the object size or beam preparation. But with the new microslit system it is possible to gain this resolution at sufficient beam current for hydrogen microscopy.

3.5 Scattering characteristics

So far we have not been able to validate the improvement of the microprobe resolution. However, we investigated the scattering characteristics of the new microprobe slit tips made of mechanically lapped tungsten [2] compared to the slits using a nearly atomically flat Si-wafer [6]. For this we have used nuclear track detectors [11], which have been placed at the single ion detection system of SNAKE after a kapton exit window [8]. First results show, that parasitical scattering effects on the slit surface of the new microslits are in the same range as with the old slits.

4 Conclusion and perspective

The system withstands a beam current of 8.7 µA at 20 MeV protons and therefore a power input of 175 W. Slit temperature is kept stable via feedback control at a slip top temperature of 100 °C with beam on and off, hence maintaining slit aperture to a precision of better than 2 µm between beam on and off times.
Furthermore, the slits were successfully tested as current feedback slits for tandem voltage control at currents up to 5 µA.
The surface roughness and thus scattering characteristics of the tungsten slit tip with large curve radius have been investigated with nuclear track detectors [11]. First results show, the higher surface roughness of the tungsten does not affect the scattering effects on the slit surface significantly.
With the new high brightness MultiCUSP ion source [3] in combination with the new microbeam slit system, the high beam brightness of $B \approx 2.8\,\mu A/(mm^2\,mrad^2\,MeV)$ at the tandem injection can be transported into SNAKE with a brightness loss of 25 % only. Therefore a higher lateral resolution of theoretically < 280 nm is possible, but the beam size is limited by parasitic effects and still some lens aberrations to ≈ 320 nm [7]. However, with the new microslit system we can achieve higher resolution not only with single ion detection setup [8, 7], but also with currents up to $I_{exp} = 100$ pA for material analysis [5]. Anyway we still have a loss of brightness of up to a factor of 10 on the low energy stage which is subject for improvements in future.

References

[1] T. Vallentin. Design und Simulation eines temperaturstabilisierten Schlitzsystems für den Transport eines hochbrillanten Protonen-Mikrostrahls. bachelor thesis. Universität der Bundeswehr München, Neubiberg, Germany (2012).

[2] T. Vallentin. Planung des Aufbaus eines temperaturstabilisierten Schlitzsystems für den Transport eines hochbrillanten Protonen-Mikrostrahls. project thesis. Universität der Bundeswehr München, Neubiberg, Germany (2013).

[3] M. Moser, P. Reichart, W. Carli, C. Greubel, K. Peeper, P. Hartung, G. Dollinger. High brilliance multicusp ion source for hydrogen microscopy at SNAKE. Nuclear Instruments and Methods in Physics Research B, 273, 226 - 230 (2012).

[4] P. Reichart, G. Datzmann, A. Hauptner, R. Hertenberger, C. Wild, G. Dollinger. Three-dimensional hydrogen microscopy in diamond. Science 306, 1537 - 1540 (2004).

[5] P. Reichart, G. Dollinger, A. Bergmaier, G. Datzmann, A. Hauptner, H.-J. Körner. Sensitive 3D hydrogen microscopy by proton proton scattering. Nuclear Instruments and Methods in Physics Research B, 197, 134 - 149 (2002).

[6] O. Schmelmer, G. Dollinger, G. Datzmann, C. Goeden, H.-J. Körner. A novel high precision slit system. Nuclear Instruments and Methods in Physics Research B, 158, 107 - 112 (1999).

[7] G. Datzmann. Aufbau und Charakterisierung des Hochenergie Rasterionenmikroskops SNAKE. phd thesis. Technische Universität München, Germany (2002).

[8] A. Hauptner, T. Cremer, M. Deutsch, S. Dietzel, G.A. Drexler, C. Greubel, V. Hable, R. Krücken, R. Löwe, H. Strickfaden, G. Dollinger and A.A. Friedl. Irradiation of Living Cells with Single Ions at the Ion Microprobe SNAKE. Acta Physica Polonica A, 109, 273 - 278 (2006).

[9] G. Hinderer, G. Dollinger, G. Datzmann, H.J. Körner. Design of the new superconducting microprobe system in Munich. Nuclear Instruments and Methods in Physics Research B, 130, 51 - 56 (1997).

[10] G. Dollinger, P. Maier-Komor. Stripper foil requirements for optimum ion transmission at the Munich MP-tandem. Nuclear Instruments and Methods in Physics Research A, 282, 153 - 160 (1989).

[11] J.-M. Osinga, M.S. Akselrod, R. Herrmann, V. Hable, G. Dollinger, O. Jäkel, S. Greilich. High-accuracy fluence determination in ion beams using fluorescent nuclear track detectors. Radiation Measurements, 56, 294 - 298 (2013).

[12] R.W. Francis, W.L. Worrell. Journal of The Electrochemical Society, Volume 123, Issue 3, 430 - 433 (1976).

[13] M.B.H. Breese, D.N. Jamieson and P.J.C. King. Materials Analysis with a Nuclear Microprobe. Wiley, New York (1996).

[14] R. Szymanski, D.N. Jamieson. Ion source brightness and nuclear microprobe applications. Nuclear Instruments and Methods in Physics Research B, 130, 80 - 85 (1997).

Acknowledgement

I hereby thank Professor Günther Dollinger for the support and the numerous discussions and helpful tips throughout the years and months.
I also thank Patrick Reichart and Marcus Moser for the best support whenever I had the need for it, your help, your critics and your continuous encouragement for my work and my studies. It was a great pleasure to work with you both and I am very proud to had the possibility to assist you at SNAKE.
I also want to acknowledge the work of Stephan Eschbaumer, Christoph Greubel and Tobias Haase, who contributed to this project with their constructions, helpful ideas and analysis.
Last but not least, I want to express my gratitude supremely to my parents Klaus and Antonie Vallentin as well as to my fiancé Anne Elliger for your affectionate and cordial support in my study- and freetime. Like a good comrade, you have been watching my '6' continuously and kept me staying on my path.